

# Beyond Fluorescent Proteins: Hybrid and Bioluminescent Indicators for Imaging Neural Activities

Anqi Wang,<sup>†,§</sup> Jiesi Feng,<sup>‡,§</sup> Yulong Li,<sup>\*,‡,§</sup> and Peng Zou<sup>\*,†,§</sup> 

<sup>†</sup>College of Chemistry and Molecular Engineering, Synthetic and Functional Biomolecules Center, Beijing National Laboratory for Molecular Sciences, Key Laboratory of Bioorganic Chemistry and Molecular Engineering of Ministry of Education, Peking University, Beijing 100871, China

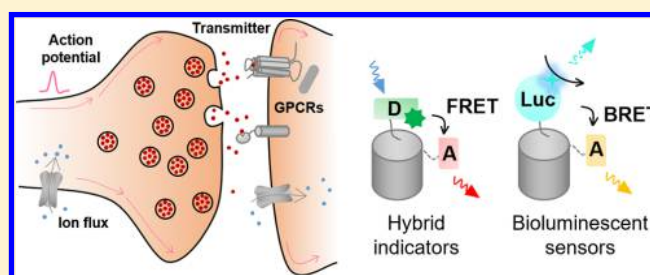
<sup>‡</sup>State Key Laboratory of Membrane Biology, School of Life Sciences, Peking University, Beijing 100871, China

<sup>§</sup>Peking-Tsinghua Center for Life Sciences, PKU-IDG/McGovern Institute for Brain Research, Peking University, Beijing 100871, China

## Supporting Information

**ABSTRACT:** Optical biosensors have been invaluable tools in neuroscience research, as they provide the ability to directly visualize neural activity in real time, with high specificity, and with exceptional spatial and temporal resolution. Notably, a majority of these sensors are based on fluorescent protein scaffolds, which offer the ability to target specific cell types or even subcellular compartments. However, fluorescent proteins are intrinsically bulky tags, often insensitive to the environment, and always require excitation light illumination. To address these limitations, there has been a proliferation of alternative sensor scaffolds developed in recent years, including hybrid sensors that combine the advantages of synthetic fluorophores and genetically encoded protein tags, as well as bioluminescent probes. While still in their early stage of development as compared with fluorescent protein-based sensors, these novel probes have offered complementary solutions to interrogate various aspects of neuronal communication, including transmitter release, changes in membrane potential, and the production of second messengers. In this Review, we discuss these important new developments with a particular focus on design strategies.

**KEYWORDS:** Biosensors, protein engineering, fluorescence imaging, bioluminescence



## INTRODUCTION

A long-standing challenge in the field of neuroscience has been understanding how complex behaviors such as learning and memory arise from the interactions between membrane potential dynamics, synaptic transmitter release, and signaling via intracellular second messengers. In the presynaptic neuron, an action potential propagates along the axon to the presynaptic terminal, triggering the influx of calcium ions ( $\text{Ca}^{2+}$ ) through voltage-gated  $\text{Ca}^{2+}$  channels, leading to the release of neurotransmitters via vesicle fusion. These neurotransmitters then diffuse across the narrow synaptic cleft, activating receptors on presynaptic and/or postsynaptic neurons, thereby changing membrane potential and/or initiating the production of intracellular second messengers. Fully understanding the mechanisms by which information is processed in the intact brain requires the ability to monitor each of these signals with high spatial and temporal resolution. Compared to traditional approaches such as patch-clamp recording of membrane potential and using voltammetry to measure neurotransmitter release, imaging neural activities with optical probes offers many important advantages; for example, these probes can be noninvasive, cell-type specific, have high

molecular specificity, are relatively easy to use, and provide signal amplification.

Since the discovery, cloning, and development of fluorescent proteins (FPs) at the end of the last century,<sup>1–3</sup> a majority of optical sensors have been constructed using these FPs as a scaffold; these probes usually use an analyte binding-induced conformational change to modulate the optical properties of the FP, including absorption spectrum, fluorescence quantum yield, emission wavelength etc. These sensors have been reviewed quite thoroughly in several recent publications and will not be discussed in detail here.<sup>4–6</sup> Despite their successful use in a variety of applications, FP-based sensors have several inherent limitations: they are typically less bright and less photostable compared to synthetic fluorophores;<sup>7</sup> their bulky size can limit their dynamic range;<sup>8</sup> and the need to provide excitation light can give rise to background autofluorescence from the sample (with the exception of near-infrared fluorescent proteins).<sup>9</sup> To overcome these limitations, several

**Received:** November 17, 2017

**Accepted:** February 26, 2018

**Published:** February 26, 2018

Table 1. Overview of the Hybrid and Bioluminescent Indicators Discussed in This Review<sup>a</sup>

| indicator name                             | analyte                       | optical reporter            | sensitivity<br>$\Delta F/F_0$ (%) | affinity ( $K_d$ ) | cell type tested                               | ref   |
|--|-------------------------------|-----------------------------|-----------------------------------|--------------------|--|-------|
| <b>neurotransmitter sensors</b>            |                               |                             |                                   |                    |  |       |
| EOS  | glutamate                     | Oregon Green 488            | 21                                | 148 nM             | HeLa   | 12    |
| K716A-EOS                                  | glutamate                     | Oregon Green 488            | 29                                | 174 nM             | in vitro                                       | 15    |
| L401C-EOS                                  | glutamate                     | Oregon Green 488            | 48                                | 1.57 $\mu$ M       | in vitro                                       | 15    |
| eEOS                                       | glutamate                     | AX488 II                    | 500                               | 66 $\mu$ M         | in vitro/neuronal cell surface                 | 17    |
| A <sub>2A</sub> -Flash3-CFP                | adenosine                     | FLAsH                       | 10                                | N.A.               | HEK293   | 20    |
| A <sub>2A</sub> -AR-Flash/CFP              | norepinephrine                | FLAsH                       | 20                                | N.A.               | HEK293   | 20    |
| $\beta_{2A}$ R-4Cys(250–259)-CFP           | epinephrine                   | FLAsH                       | <1                                | N.A.               | HEK293   | 21    |
| M-type AChR-based FRET                     | acetylcholine                 | FLAsH                       | <10                               | 0.5–1.5 $\mu$ M    | HEK293   | 22–24 |
| Snifit-iGluR5                              | glutamate                     | DY-547/Cy5                  | 93                                | 15 $\mu$ M         | HEK293   | 26    |
| GABA-Snifit                                | GABA                          | AlexaFluor488/Cy5           | 80                                | 100 $\mu$ M        | HEK293   | 27    |
| ACh-Snifit                                 | acetylcholine                 | Cy3/Cy5                     | 65                                | 10 mM              | HEK293   | 32    |
| ST-mGlu2                                   | glutamate                     | Lumi4-Tb/Green              | 80                                | 100 $\mu$ M        | HEK293   | 33    |
| $\beta$ 2AR-RLuc + YFP- $\beta$ -arrestin2 | epinephrine                   | coelenterazine or DeepBlueC | 8                                 | 30 nM              | HEK293   | 34    |
| <b>metal ion sensors</b>                   |                               |                             |                                   |                    |  |       |
| SNAP1-Indo-1                               | Ca <sup>2+</sup>              | Indo-1                      | 1580                              | 570 nM             | in vitro                                       | 42    |
| SNAP3-Indo-1                               | Ca <sup>2+</sup>              | Indo-1                      | 950                               | 290 nM             | in vitro                                       | 42    |
| BOCA-1-SNAP                                | Ca <sup>2+</sup>              | BOCA-1                      | 18000                             | 200 nM             | in vitro                                       | 43    |
|  |                               |                             | 300–500                           | N.A.               | CHO-K1   | 43    |
| SNAP-Fura-2FF-1                            | Ca <sup>2+</sup>              | Fura-2FF                    | 1170                              | 4.30 $\mu$ M       | in vitro                                       | 44    |
| GFP-aequorin                               | Ca <sup>2+</sup>              | GFP/aequorin                | ~5000                             | N.A.               | in vitro                                       | 47    |
| BRAC                                       | Ca <sup>2+</sup>              | Rluc8/Venus                 | 60                                | 1.9 $\mu$ M        | in vitro                                       | 50    |
| CNL (Ca <sup>2+</sup> )                    | Ca <sup>2+</sup>              | Rluc8/mTurquoise2           | N.A.                              | N.A.               | HeLa, imaging Ca <sup>2+</sup> spikes          | 52    |
| ONL (Ca <sup>2+</sup> )                    | Ca <sup>2+</sup>              | RLuc8.6/mKusabiraOrange2    | N.A.                              | N.A.               | HeLa, imaging Ca <sup>2+</sup> spikes          | 52    |
| GeNL (Ca <sup>2+</sup> )                   | Ca <sup>2+</sup>              | NLuc/mNeonGreen             | 500                               | 60–520 nM          | HeLa   | 53    |
| CalfluxVTN                                 | Ca <sup>2+</sup>              | NanoLuc/Venus               | 1100                              | 480 nM             | in vitro                                       | 56    |
| ZP1-AGT                                    | Zn <sup>2+</sup>              | ZP1                         | 270                               | N.A.               | in vitro (2 equiv of Zn <sup>2+</sup> )        | 62    |
| ZIMIR-HaloTag                              | Zn <sup>2+</sup>              | ZIMIR                       | 1500                              | 126 nM             | in vitro                                       | 64    |
| BLZinCh-3                                  | Zn <sup>2+</sup>              | NanoLuc/Cerulean/Citrine    | 50                                | 15.6 pM            | in vitro/HeLa                                  | 65    |
| <b>ROS/RNS sensors</b>                     |                               |                             |                                   |                    |  |       |
| SNAP-Peroxy-Green                          | H <sub>2</sub> O <sub>2</sub> | Peroxy-Green                | 3200                              | N.A.               | in vitro (1 mM H <sub>2</sub> O <sub>2</sub> ) | 73    |
| SO <sub>3</sub> H-APL                      | hROS                          | luciferin                   | 15000                             | N.A.               | Neutrophil                                     | 76    |
|  |                               |                             | ~450                              | N.A.               | Rat  | 76    |
| TMR-NO-SNAP                                | NO                            | TMR                         | 1900                              | N.A.               | in vitro                                       | 74    |
|  |                               |                             | >4000                             | N.A.               | COS-7 (20 equiv of NO)                         | 74    |
| DAL  | NO                            | luciferin                   | 4100                              | N.A.               | in vitro                                       | 75    |
| <b>voltage sensors</b>                     |                               |                             |                                   |                    |  |       |
| PLAP-activated hemicyanine                 | voltage                       | di-4-ANEPPS                 | 10                                |                    | HEK293   | 78    |
| FLOX4                                      | voltage                       | fluorescein                 | 22–34                             |                    | 1321N astrocytoma cell line                    | 79    |
| hVOS                                       | voltage                       | eGFP                        | 34                                |                    | HEK293   | 81    |
|  |                               |                             | 4.2                               |                    | neuron   | 81    |
| hVOS 2.0                                   | voltage                       | CeFP                        | 26                                | per 100 mV         | PC12   | 84    |
|  |                               |                             | 10                                |                    | neuron   | 84    |
| Flare1                                     | voltage                       | Cy3                         | 35                                |                    | HEK293   | 93    |
| LOTUS-V                                    | voltage                       | NanoLuc/Venus               | 21                                |                    | HEK293   | 97    |

<sup>a</sup>N.A., not available; for other definitions, please see the main text.

hybrid indicators and bioluminescent probes have been developed, thereby providing researchers with a set of tools that complement existing FP-based sensors.

Hybrid indicators combine the advantages of a synthetic small molecule with a genetically encoded protein scaffold. While synthetic probes are bright, photostable, and small in size, the protein scaffold can be readily targeted to genetically specified cell subtypes and/or subcellular compartments. In sensors that rely upon Förster resonance energy transfer (FRET), the small size of the synthetic dye provides close proximity between the donor and acceptor, which may increase FRET efficiency and the sensor's dynamic range. Unlike hybrid

indicators and FPs, bioluminescent probes do not require excitation light; this advantage eliminates background autofluorescence and the possibility of phototoxicity, and it allows the indicator to be easily paired with an optogenetic actuator.

In this Review, we discuss the design and characterization of these indicators, as well as their applications for monitoring neurotransmitters, metal ions, reactive oxygen and reactive nitrogen species (ROS/RNS), and membrane potential. We have summarized the sensitivity, kinetics and photophysical properties of these sensors in Table 1 and Supplementary Table 1.

## NEUROTRANSMITTER SENSORS

To date, several dozen neurotransmitters and neuromodulators have been identified in the mammalian nervous system. The release of these neurotransmitters/neuromodulators is spatially specific, temporally dynamic, and tightly regulated in the healthy brain. On the other hand, impaired neurotransmitter and/or neuromodulator transmission can contribute to a wide range of neurological disorders, including schizophrenia,<sup>10</sup> depression, and addiction.<sup>11</sup> Therefore, the ability to measure the spatial and temporal dynamics of these signaling molecules with high sensitivity and specificity can greatly increase our ability to understand their mechanism of action.

Historically, neurotransmitter receptors have often served as the starting point when engineering a sensor. Hybrid neurotransmitter sensors have been built by chemically modifying these receptors or by modifying the receptor's ligand-binding domain. For example, the glutamate-binding S1S2 domain in the GluA2 subunit of the AMPA receptor was used as the scaffold for constructing the hybrid glutamate optical sensor EOS.<sup>12</sup> To take advantage of the conformational change induced by glutamate binding, the organic fluorophore Oregon Green 488 was conjugated to an engineered, surface-exposed cysteine residue (S403C mutation) in the S1S2 domain (Figure 1A). When this sensor is expressed in HeLa cells, glutamate binding increases the sensor's peak fluorescence by 21% ( $\Delta F/F_0$ ), with a dissociation constant ( $K_d$ ) of 148 nM, which provides slightly higher affinity than the GluR4 S1S2 ( $\sim 500$  nM<sup>13</sup>). In comparison, the glutamate concentration in the nervous system ranges from nanomolar to millimolar, depending on neural activities.<sup>14</sup> Additional mutations in the sensor shifted the  $K_d$  and/or increased the sensitivity for glutamate.<sup>15,16</sup> For example, the K716A-EOS version has similar affinity for glutamate ( $K_d = 174$  nM), but higher sensitivity (peak  $\Delta F/F_0 = 29\%$ ). The L401C-EOS version, which conjugates with Alexa Fluor 488, has a 10-fold reduction in affinity ( $K_d = 1.57$   $\mu$ M) and even higher sensitivity to glutamate (peak  $\Delta F/F_0 = 48\%$ ). These  $K_d$  and dynamic range are suitable to detect micromolar concentration of glutamate dynamics. When used to monitor glutamate release in mouse somatosensory cortical neurons in response to limb movement, the L401C-EOS sensor yielded a  $\sim 1$ –2% increase in fluorescence.<sup>15</sup> To increase the dynamic range of EOSs, Hirose et al. systematically scanned 270 amino acids in the S1S2 domain and tested various combinations of four different commercially available fluorophores.<sup>17</sup> Their efforts eventually produced the improved version, G448C-AX488 II (referred to simply as enhanced EOS, or eEOS). Purified eEOS sensor protein exhibits an impressive 2000% dynamic range with an in vitro glutamate affinity of 66  $\mu$ M. eEOS produces a 30% increase in fluorescence when used to detect glutamate release stimulated by a single action potential in neurons. Notably, eEOS has achieved a quantum yield of 0.82, which is similar to that of the parent fluorophore AX488 II. While the EOS series lay out the foundation to detect glutamate under confocal or two-photon microscopy, the requirement of labeling on the cell surface with streptavidin has limited their usage. Moreover, this method also lacks cellular resolution for in vivo imaging. The next logical step is to conjugate the sensor to cell-surface receptors or add a motif to target the sensor to the designated plasma membrane, which would provide the ability to detect cell-specific glutamate signals.

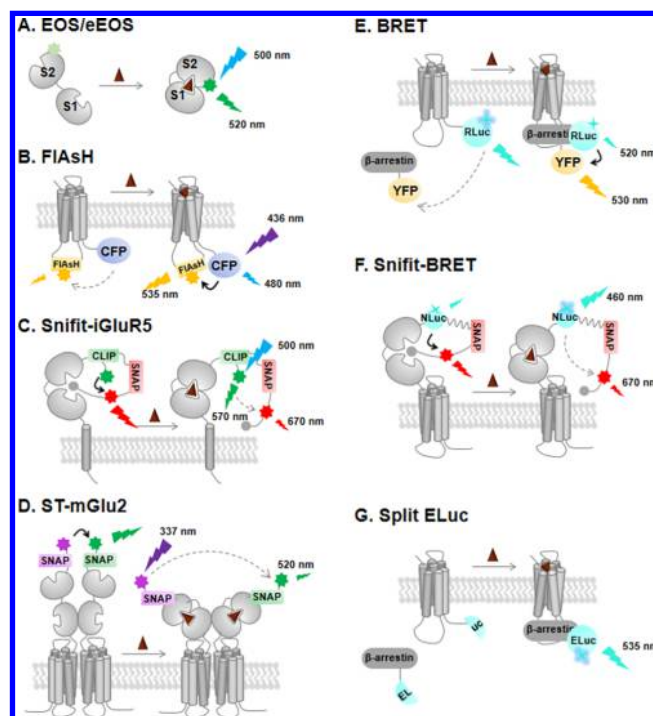


**Figure 1.** Schematic overview of currently available hybrid sensors for sensing neurotransmitters. (A) Glutamate optical sensor (EOS) and its enhanced version (eEOS).<sup>12,15,17</sup> S1S2, the subdomains of the extracellular domain in GluA2, are conjugated with Oregon Green 488 (in EOS) or AX488 II (in eEOS) (shown in green) via a cysteine mutation. (B) Hybrid FRET-based sensor using FIAsh (fluorescein with As(III) substituents at the 4'- and 5'-positions) as the donor. The FIAsh binding motif is inserted into ICL3, and CFP is attached to the receptor's C-terminus. (C) Snifit-iGluR5.<sup>28</sup> The CLIP-tag and SNAP-tag are covalently labeled with the fluorophores DY547 (in green) and Cy5 (in red), respectively. The glutamate moiety is indicated by the filled gray circle. (D) ST-mGlu2<sup>35</sup> labeled with the Lumi4-Tb as the donor (in pink) and the GFP as the acceptor (in green). (E) A BRET-based neurotransmitter sensor based on the interaction between the GPCR and  $\beta$ -arrestin2.<sup>34</sup> RLuc and its substrate (in blue) and YFP (yellow) serve as the FRET pair. (F) Snifit-like bioluminescence sensor similar to the Snifit-iGluR5 sensor shown in panel (C), except that NLuc and its substrate (in blue) serves as a BRET donor. (G) Split ELuc reporter based on the interaction between the GPCR and  $\beta$ -arrestin2.<sup>38</sup> In each panel, the brown triangle indicates a specific neurotransmitter (e.g., glutamate, epinephrine, acetylcholine, etc.). Additional details are provided in the text.

FRET can also be used to sense a conformational change in the corresponding receptor following ligand binding. When developing a FRET-based sensor, both the orientation and distance between the two fluorophores are critical. Based on the conformational change induced by a GPCR binding to its ligand, CFP and YFP (cyan and yellow fluorescent proteins, respectively) were used as the FRET pair when developing neurotransmitter sensors.<sup>18</sup> However, because the chromophore in a fluorescent protein is buried inside the  $\beta$ -barrel, the dynamic range of the FRET signal is relatively low due to distance constraints. Thus, a hybrid FRET pair was later created in which CFP was attached to the C-terminus of the receptor and the cell-permeable fluorophore FIAsh (fluorescein arsenical hairpin binder) was conjugated to a 6-amino acid peptide in the receptor's third intracellular loop (Figure 1B).<sup>19</sup> To date, hybrid FIAsh-FRET sensors based on the A2A adenosine receptor,<sup>20</sup> adrenergic receptors,<sup>20,21</sup> and muscarinic

receptors<sup>22–24</sup> have been used to detect adenosine, epinephrine, and acetylcholine, respectively, in cultured cells; however, their relatively small signal amplitude (<20%) has limited their applications. Even with the introduction of a circularly permuted CFP, this GPCR-FRET sensor did not yet achieve a signal change that exceeds 20%.<sup>24</sup> Further refinements have attempted to reduce the distance between the FRET pair by replacing CFP with a different binding motif of the red biarsenical dye ReAsH, which, unfortunately, failed to produce detectable FRET signals.<sup>25</sup> These FAsH/ReAsH-based hybrid sensors have not been used to detect neurotransmitter release *in vivo*.

The most promising and successful FRET-based hybrid neurotransmitter sensor to date is probably Snifit (SNAP-tag based indicator proteins with a fluorescent intramolecular tether). This sensor is comprised of a module for sensing the binding of a specific neurotransmitter (e.g., glutamate, GABA, etc.) fused with a reporter module containing two tandem self-labeling protein tags, SNAP-tag and CLIP-tag.<sup>26–28</sup> SNAP-tag is a 20-kDa engineered human DNA repair protein O<sup>6</sup>-alkylguanine-DNA alkyltransferase that reacts specifically with benzylguanine derivatives to covalently attach a synthetic fluorophore.<sup>29,30</sup> CLIP-tag is similar to the SNAP-tag but reacts specifically with benzylcytosine derivatives.<sup>31</sup> Together, SNAP-tag and CLIP-tag form an orthogonal labeling pair used to construct the FRET sensor. To measure glutamate, the glutamate-Snifit sensor uses the ionotropic glutamate receptor 5 (iGluR5) as the sensing module.<sup>28</sup> The CLIP-tag binds to a FRET donor (e.g., green-emitting DY-547), while the SNAP-tag binds to a synthetic ligand composed of a FRET acceptor tethered to a glutamate moiety via a short polyethylene glycol spacer (Figure 1C). In the absence of extracellular glutamate, iGluR5 binds to the glutamate moiety on the SNAP-tag ligand, forcing the Snifit sensor to adopt a closed conformation and to increase the FRET efficiency. Exogenous glutamate (for example, released from synaptic vesicles) competes with the SNAP-tag ligand for iGluR5 binding, causing a shift in the Snifit sensor's conformation, thereby reducing FRET efficiency. When expressed in HEK293 cells, the glutamate-Snifit sensor produces a peak ratiometric fluorescence signal change of 1.93ΔR, with a  $K_d$  of 15 μM for glutamate.

A GABA-Snifit reporter has also been generated using a similar strategy, with the metabotropic GABA<sub>B</sub> receptor as the sensing module.<sup>27</sup> In this sensor, the GABA analogue CGP 51783 is tethered to the SNAP-tag ligand to compete with extracellular GABA binding. When expressed in HEK293 cells, the GABA-Snifit sensor produces a peak ratiometric fluorescence change of 1.8ΔR with a  $K_d$  of 100 μM for GABA.

A third Snifit-based neurotransmitter sensor, ACh-Snifit, consists of a catalytically inactive acetylcholinesterase with a CLIP-tag and SNAP-tag.<sup>32</sup> The ACh-Snifit-Deca sensor, a variant of the ACh-Snifit sensor, produces a ratiometric fluorescence change of 1.52ΔR with a  $K_d$  of 20 mM for acetylcholine, which may not have enough sensitivity for *in vivo* imaging. Because the chemical reagents used to label the sensor are not membrane-permeable, the fluorescence signal is restricted largely to the cell membrane, thereby reducing intracellular background. For use in *in vivo* applications, Snifits should be optimized by increasing their dynamic range and by fine-tuning their affinity to correspond to physiological levels of glutamate and GABA. Moreover, the signal-to-noise ratio (SNR) of Snifit sensors can be increased by conjugating a rationally designed activatable “turn-on” fluorophore to the

SNAP-tag and CLIP-tag modules. In principle, the generic approach used to design Snifit sensors can be adapted for developing other neurotransmitter sensors using various neurotransmitter binders anchored to the plasma membrane.

Neurotransmitter sensors based on time-resolved FRET (trFRET) can produce a higher SNR compared to conventional FRET probes, as trFRET can separate a long-lived FRET signal from background noise (e.g., short-lived autofluorescence or leakage of the excitation light). trFRET has been used to probe the glutamate-induced dimerization of GluR2 subunits.<sup>33</sup> Specifically, Lumi4-Tb (a long-lived trFRET donor) and SNAP green (an acceptor dye) were conjugated to an individual GluR2 protein containing an extracellular SNAP-tag, resulting in ST-mGlu2. Binding of glutamate causes GluR2 dimerization and a corresponding trFRET signal (Figure 1D), with a peak ratiometric fluorescence signal change of approximately 1.8ΔR and a  $K_d$  for glutamate of approximately 10 μM. However, whether trFRET-based probes can be used to detect neurotransmitter release *in vivo* is currently unclear, partly due to limitations with respect to the instrumentation required; most commercially available instruments for measuring trFRET are plate readers, which is ideal for screening drugs in cultured cells *in vitro*, but not for spatially resolved imaging *in vivo*.

Another strategy that can provide a good SNR by removing unintended autofluorescence background is bioluminescent resonance energy transfer (BRET). A BRET-based reporter for measuring a neurotransmitter was generated based on the recruitment of arrestin to the C-terminus of a GPCR upon ligand binding. In this system, the BRET ratio was measured by coexpressing a cytosolic YFP-β-arrestin2 and a GPCR-linked *Renilla* luciferase reporter (RLuc), a widely used donor protein that emits bioluminescence in the blue wavelength (Figure 1E).<sup>34</sup> Ligand binding to this reporter elicits a modest (~5%) increase in the BRET ratio. An improved BRET-based reporter with a larger BRET ratio increase (15% higher than the previous generation reporter) has also been reported;<sup>35</sup> in this second-generation BRET-based reporter, the donor Venus (an enhanced version of YFP) was attached to the GPCR's C-terminus and RLuc was fused to the cytosolic β-arrestin2. In a more recently reported version, RLuc was replaced with the smaller, brighter luciferase NanoLuc (NLuc), yielding a higher SNR sensor and enabling researchers to image S1PR1 (sphingosine-1-phosphate receptor 1) activation *in vivo* in mice.<sup>36</sup> Moreover, Lucids (luciferase-based indicators of drugs) have been used to generate low-cost sensors for methotrexate and sirolimus.<sup>37</sup> The strategy employed in BRET sensors is analogous to the Snifit strategy, except the fluorophore in a Snifit sensor is replaced with a bioluminescent protein (e.g., NLuc). Thus, a Lucid sensor based on a neurotransmitter receptor (for example, a ligand-gated ion channel or GPCR) would provide a bioluminescent reporter (Figure 1F) ideally suited for the tissue-specific detection of neurotransmitters *in vivo*. In principle, a reporter could also be designed based on the protein fragment complementation assay by fusing two halves of a bioluminescent protein (e.g., luciferase) to a GPCR and an arrestin molecule (Figure 1G); neurotransmitter binding would then result in the assembly of a functional luciferase molecule.<sup>38</sup>

## ■ METAL ION SENSORS

Ca<sup>2+</sup> is arguably the most important intracellular messenger in neuroscience.<sup>39</sup> In response to action potentials, the local

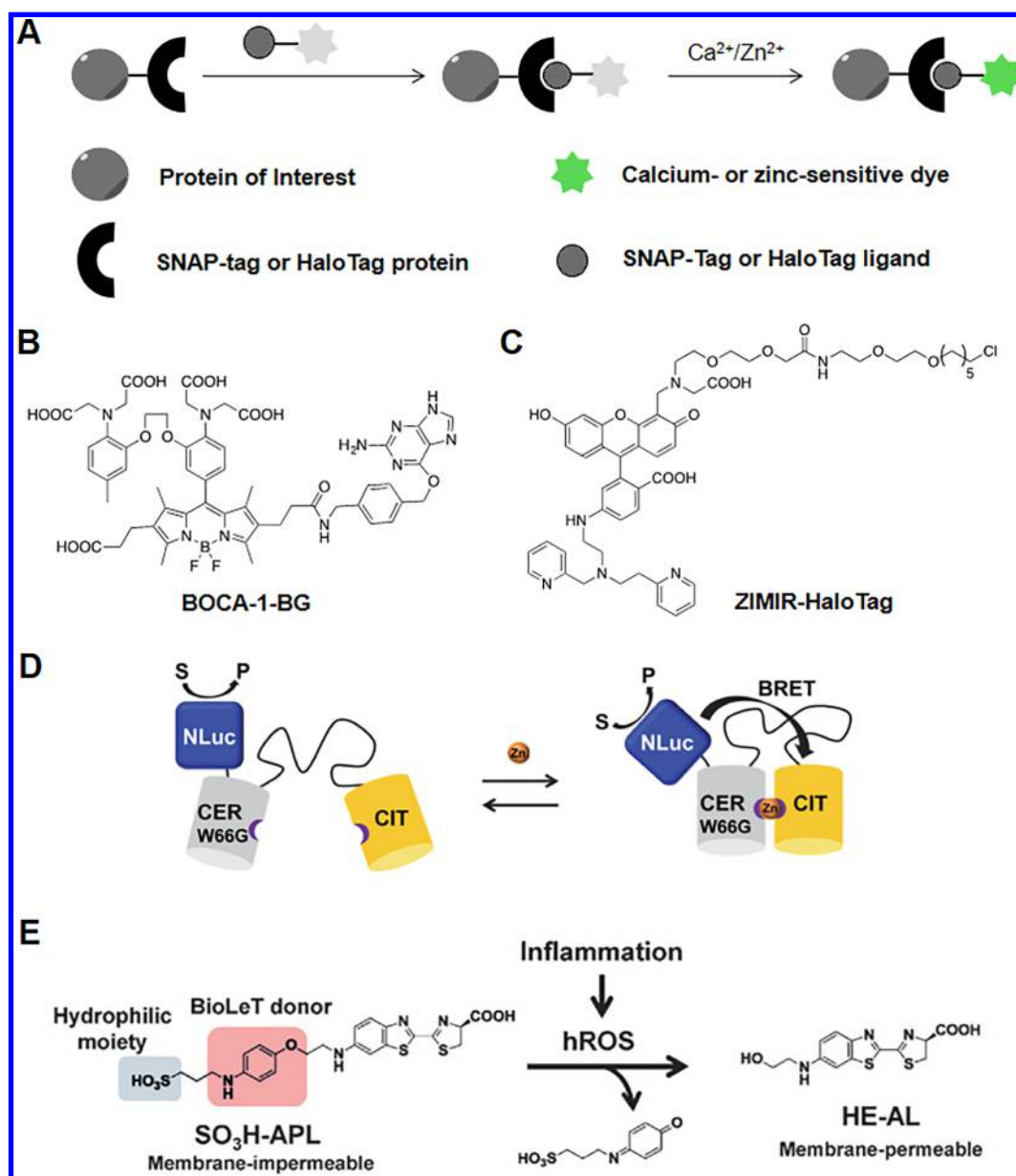


**Figure 2.** Schematic diagrams and applications for hybrid and bioluminescent sensors used to detect metal ions and ROS/RNS. (A) SNAP-tag and HaloTag mediates cell-specific and/or subcellular targeting of  $\text{Ca}^{2+}/\text{Zn}^{2+}$  indicators. (B) Chemical structure of BOCA-1-BG, which consists of a  $\text{Ca}^{2+}$ -binding moiety linked to a BODIPY fluorophore and the SNAP-tag ligand BG.<sup>43</sup> (C) Chemical structure of ZIMIR-HaloTag, which contains a fluorescein molecule linked to  $\text{Zn}^{2+}$ -chelating molecule and the HaloTag ligand.<sup>64</sup> (D) Structure of BRET  $\text{Zn}^{2+}$  sensor, BLZinCh-3.<sup>65</sup> (Reproduced from ref 65. Copyright 2016 American Chemical Society.) (E) The luciferin moiety of  $\text{SO}_3\text{H}$ -APL is caged by the aniline group, which is removed upon reaction with hROS, rendering the dye brightly luminescent.<sup>76</sup>

calcium concentration could reach hundreds of micromolars.<sup>40</sup> The study of  $\text{Ca}^{2+}$  signaling was revolutionized in the early 1980s by the development of chemical  $\text{Ca}^{2+}$  indicators by Roger Tsien and colleagues; indeed, many of these indicators, including Fura-2 and Indo-1, are still used widely today.<sup>41</sup> To provide genetic targeting for these indicators, a series of hybrid  $\text{Ca}^{2+}$  sensors were later developed by Johnsson and colleagues by generating SNAP-tag fusion proteins (Figure 2A). For example, SNAP-1-Indo-1, which was developed in 2009, produces a 15.8-fold increase in the fluorescence emission ratio (405/485 nm) in response to  $\text{Ca}^{2+}$ , with a  $K_d$  of 570 nM.<sup>42</sup> Other dyes with a rapid, sensitive  $\text{Ca}^{2+}$  response, for example, the BODIPY-based  $\text{Ca}^{2+}$  indicator BOCA-1 and Fura-2FF, have also been used as SNAP-tag ligands in the generation of hybrid

sensors (Figure 2B).<sup>43,44</sup> Among these hybrid sensors, BOCA-1-BG produces a remarkable 180-fold increase in fluorescence intensity upon binding  $\text{Ca}^{2+}$ , with a  $K_d$  of 200 nM, and has been used to report local changes in  $\text{Ca}^{2+}$  levels in the nucleus and cytosol of mammalian cells.<sup>43</sup> This dynamic range is about 3-fold higher than fluorescent protein-based calcium indicator GCaMP6s ( $F_{\text{max}}/F_{\text{min}} = 63.2$ ).<sup>45</sup>

As discussed above, bioluminescent  $\text{Ca}^{2+}$  indicators are well-suited for in vivo imaging due to their low autofluorescence background. Aequorin is a natural  $\text{Ca}^{2+}$ -sensitive bioluminescent protein, but its luminescence is quite dim.<sup>46</sup> Fusing this protein with GFP dramatically enhances the luminescence intensity by  $\sim 50$ -fold due to the highly efficient BRET mechanism.<sup>47</sup> However, the relatively slow turnover rate of

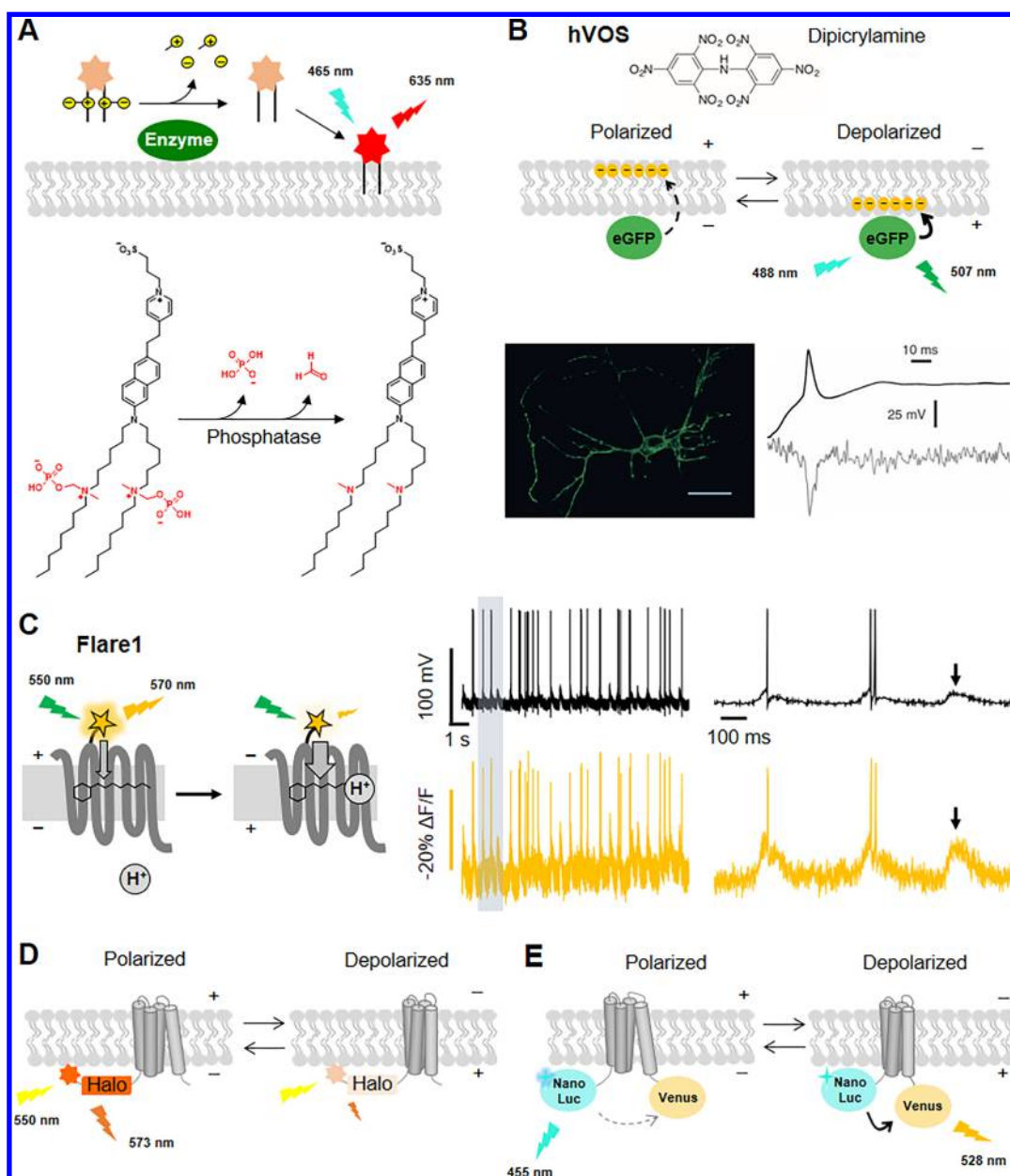


**Figure 3.** Hybrid and bioluminescent voltage indicators. (A) PLAP-activated ANEPPS dye. Membrane-targeted alkaline phosphatase locally activates the voltage-sensitive dye to achieve cell-specific staining. Reproduced from ref 78. Copyright 2010 American Chemical Society. (B) Hybrid voltage sensor (hVOS) consisting of a membrane-anchored eGFP (green) and a membrane-mobile dipicrylamine (orange), which upon membrane depolarization, translocates across the lipid bilayer and modulates the eGFP fluorescence. Left: fluorescence image of a rat hippocampal neuron expressing membrane anchored eGFP in a hVOS indicator (scale bar: 50  $\mu\text{m}$ ). Right: hVOS reports neuronal action potential after averaging eight individual traces. Reproduced from Chanda et al.<sup>31</sup> (C) Hybrid voltage indicator Flare1 reports simulated action potential waveforms in single trial measurements in HEK293T cells. Reproduced from Xu et al.<sup>93</sup> (D) VSD-HaloTag-TMR uses the environment-sensitive dye tetramethylrhodamine (TMR) to detect the conformational change of VSD in response to depolarization. (E) LOTUS-V uses NanoLuc (blue) as the BRET donor and Venus (yellow) as the acceptor. Membrane voltage regulates the BRET efficiency via conformational changes in the VSD.<sup>97</sup>

aequorin limits its application in long-term imaging.<sup>48</sup> In 2010, Nagai et al. fused an enhanced *Renilla* luciferase donor (RLuc8)<sup>49</sup> and a yellow FP acceptor (Venus) to a  $\text{Ca}^{2+}$ -sensing domain comprised of calmodulin and M13 (CaM-M13). The resulting sensor, called BRAC, utilizes the  $\text{Ca}^{2+}$  binding-induced conformational change to modulate the energy transfer efficiency, with a peak response of 60%.<sup>50</sup> BRAC has been used to visualize  $\text{Ca}^{2+}$  dynamics at the single-cell level with temporal resolution of 1 Hz. Iterative optimization of the spatial arrangement (e.g., linker truncation) and the photophysical properties (e.g., brightness and spectral overlap) of the

bioluminescent donor and FP acceptor led to the development of Nanolantern, a novel Venus-RLuc8 (S275G) fusion protein with enhanced BRET efficiency.<sup>51</sup> Inserting the CaM-M13 domain into a nonstructural loop in the RLuc8 moiety of Nanolantern yielded the indicator Nanolantern ( $\text{Ca}^{2+}$ ), which has a peak signal change of 300% upon binding  $\text{Ca}^{2+}$ .<sup>51</sup> Subsequently, cyan and orange color variants of Nanolantern (CNL ( $\text{Ca}^{2+}$ ) and ONL ( $\text{Ca}^{2+}$ )), and green enhanced NanoLantern (GeNL ( $\text{Ca}^{2+}$ )) have also been engineered, thus greatly expanding the spectrum of bioluminescent  $\text{Ca}^{2+}$  imaging.<sup>52,53</sup> Notably, CNL ( $\text{Ca}^{2+}$ ) and ONL ( $\text{Ca}^{2+}$ ) have

enabled simultaneous bioluminescent imaging of histamine-stimulated calcium spikes in the mitochondria and the nucleus in cultured HeLa cells.<sup>52</sup> Recently, Johnson et al. inserted the Ca<sup>2+</sup>-sensing domain of troponin C between Venus and the enhanced luciferase NanoLuc;<sup>54,55</sup> the resulting indicator, called CalfluxVTN, has a >11-fold change in BRET ratio upon binding Ca<sup>2+</sup>, with a K<sub>d</sub> of 480 nM.<sup>56</sup> Notably, because luminescence-based imaging does not require excitation light, both the Nanolantern (Ca<sup>2+</sup>) indicator and CalfluxVTN can be paired with optogenetic actuators to provide all-optical interrogation of neuronal activity; this strategy was used recently to measure the activity of rat hippocampal neurons.<sup>51,56</sup> Future improvements in BRET-based Ca<sup>2+</sup> sensor will likely include the development of brighter luciferases, higher BRET efficiency through protein engineering, and a wider range of wavelengths.<sup>53,57</sup>

Like Ca<sup>2+</sup>, zinc (Zn<sup>2+</sup>) is an important signaling ion in the central nervous system. The basal Zn<sup>2+</sup> concentrations are typically on the order of 10 nM in the extracellular space and 1 nM in intracellular compartments.<sup>58</sup> Altered Zn<sup>2+</sup> signaling in the hippocampus has been associated with several neurological disorders, including depression, memory deficits, and cognitive decline.<sup>58–60</sup> Like the hybrid Ca<sup>2+</sup> sensors discussed above, synthetic Zn<sup>2+</sup> indicators can be targeted to specific cells and/or subcellular compartments by conjugating the sensor with a protein tag such as SNAP-tag or HaloTag, an engineered protein-labeling tag derived from mutant dehalogenase, which covalently binds its synthetic ligand to anchor the fluorophore at its surface.<sup>61</sup> For example, SNAP-tag labeling was used for organelle-specific monitoring of Zn<sup>2+</sup> levels with the Zn(II)-sensitive ZP1 sensor, which reported a ~2.7-fold increase in fluorescence upon binding Zn<sup>2+</sup>.<sup>62</sup> Recently, Li et al. reported the development of a HaloTag-conjugated Zn<sup>2+</sup> probe called ZIMIR<sup>63</sup> which has a 15-fold change in fluorescence upon binding Zn<sup>2+</sup> and a K<sub>d</sub> of 126 nM (Figure 2C).<sup>64</sup> In the Zn<sup>2+</sup>-free state, ZIMIR has a low fluorescence quantum yield due to intramolecular photoinduced electron transfer (PeT) between its amino group and the fluorescein moiety. Upon binding Zn<sup>2+</sup>, a coordinate bond forms, occupying the amino group's lone pair electrons, thus restoring ZIMIR fluorescence.<sup>63</sup> The large dynamic range of ZIMIR-HaloTag has enabled researchers to directly visualize the release of Zn<sup>2+</sup> in pancreatic islet beta cells.<sup>64</sup> Recently, NanoLuc was fused with the FRET-based Zn<sup>2+</sup> sensor eZinCh-2; the resulting bioluminescent probe was then used to sense Zn<sup>2+</sup> in individual living cells, producing a 50% increase in BRET efficiency upon binding Zn<sup>2+</sup>, with extremely high affinity for Zn<sup>2+</sup> (K<sub>d</sub> = 15 pM) (Figure 2D).<sup>65</sup>

## ■ ROS/RNS SENSORS

In a healthy adult, the brain represents approximately 2% of the body's total weight, yet this organ consumes up to 20% of all oxygen consumed by the entire body. Respiration fuels the formation of reactive oxygen species (ROS); however, ROS are not merely a byproduct of the brain's metabolic activity, but are important signaling molecules in the brain.<sup>66</sup> For example, hydrogen peroxide (H<sub>2</sub>O<sub>2</sub>) regulates a wide range of neurophysiological processes, including synaptic plasticity, neurotransmission, and ion channel activity.<sup>67–69</sup> Like ROS, reactive nitrogen species (RNS) such as nitric oxide (NO) also play important roles in the mammalian nervous system, including neuronal proliferation/differentiation and synaptic plasticity.<sup>70–72</sup>

The SNAP-tag fusion protein has been used to target ROS/RNS sensors to specific subcellular regions. For example, Chang et al. developed SNAP-Peroxy-Green, a boronate-caged fluorescein molecule covalently linked to a SNAP-tag ligand.<sup>73</sup> SNAP-Peroxy-Green responds selectively to H<sub>2</sub>O<sub>2</sub>, but not to other biologically relevant ROS, through an uncaging reaction. Xiao et al. generated an NO-sensitive probe by connecting an “*o*-phenylenediamine-locked” rhodamine spirolactam-based probe to a SNAP-tag ligand, yielding TMR-NO-SNAP.<sup>74</sup> In its spirocyclic form, rhodamine is nonfluorescent; the addition of NO induces opening of the ring and restores the brightly fluorescent rhodamine, producing a 19-fold increase in fluorescence at 564 nm.<sup>74</sup>

Recently, Urano et al. used the synthetic “caged luciferin” strategy to report NO and highly reactive oxygen species (hROS) *in vivo* in rats.<sup>75,76</sup> The NO probe, diamino-phenylpropyl-AL (DAL), contains a luciferin moiety linked to a diaminophenyl group, which serves as a PeT donor to efficiently quench luciferase-dependent luminescence. Reaction with NO destroys the diaminophenyl group, resulting in a ~41-fold increase in luminescence.<sup>75</sup> This so-called bioluminescent enzyme-induced electron transfer (BioLeT) approach was also used to detect hROS, with an hROS-sensitive alkyloxyaniline moiety serving as the PeT donor (Figure 2E); this probe, called SO<sub>3</sub>H-APL, provides an excellent dynamic range of ~150-fold in cultured neutrophils and has been used to monitor hROS production *in vivo* in rats.<sup>76</sup>

## ■ MEMBRANE POTENTIAL SENSORS

Synthetic voltage-sensitive dyes can be targeted to specific cell populations via enzyme-mediated uncaging.<sup>77</sup> Fromherz and Ng introduced two phosphonoxyethylammonium zwitterions into the alkyl chains of a voltage-sensitive hemicyanine dye to create a hydrophilic precursor molecule that does not stain the cell membrane. The genetically encoded component is an alkaline phosphatase targeted to the cell surface, where it enzymatically cleaves the zwitterion moiety, converting the precursor molecule to a voltage-sensing molecule that can stain the cell membrane (Figure 3A).<sup>78</sup> Inducing a transient membrane depolarization with paired field-stimulation electrodes revealed that this sensor's fluorescence increases by approximately 10% per 100 mV change in membrane potential.<sup>78</sup> However, this tool has not been used in neurons.

The first hybrid indicator of membrane potential was developed more than two decades ago by González and Tsien,<sup>79</sup> prior to the dawn of FP-based genetically encoded voltage indicators.<sup>80</sup> This first-generation indicator used FRET as the voltage-sensing mechanism, a lipophilic oxonol derivative as the acceptor, and a fluorophore-conjugated lectin (wheat germ agglutinin) as the donor. The lectin donor is membrane-impermeant and stains the outer leaflet of the cell membrane by binding to glycoproteins; in contrast, the oxonol acceptor molecules can enter the plasma membrane. At resting membrane potentials, the negatively charged oxonol molecules localize primarily near the outer leaflet and quench the lectin fluorescence. Upon membrane depolarization, however, the oxonol molecules are redistributed to the inner leaflet, increasing the distance between donor and acceptor by ~4 nm, significantly reducing FRET efficiency. Using this system, the fluorescence signal changes by as much as 34% in response to a 100 mV depolarization. Unfortunately, however, this indicator was tested in fibroblasts, cardiac myocytes, and neuroblastoma cells, but not in primary neurons. In addition,

the protein component, wheat germ agglutinin, was not genetically encoded, thus limiting its application.

Building upon this pioneering work, Bezanilla and colleagues created an improved hybrid voltage sensor (hVOS) in 2005.<sup>81</sup> Instead of staining cells with a fluorophore-conjugated lectin, GFP was anchored to the membrane using a farnesylation motif. The synthetic lipophilic dye dipicrylamine (DPA) was used as the voltage-sensing, membrane-mobile quencher. Like oxonol, the negatively charged DPA molecules move from the outer membrane leaflet to the inner leaflet upon depolarization. Fluorescence emitted from GFP is used to monitor the localization of DPA, thus indirectly reporting membrane potential (Figure 3B). When expressed in HEK293 cells, this second-generation hybrid sensor has sub-millisecond (0.54 ms) resolution and high sensitivity, with a change in fluorescence up to 34% in response to a 100-mV depolarization. Interestingly, the sensor's voltage sensitivity is considerably lower in cultured hippocampal neurons, producing only a 4.2% change in fluorescence in response to a 100-mV depolarization. Nevertheless, this hVOS has proved useful for tracking action potential spikes in individual neurons in both cultured cells and brain slices (Figure 3B).<sup>81,82</sup>

Several FP-DPA pairs have also been evaluated. Due to its improved spectral overlap with DPA, cyan fluorescent protein (CFP) provides better sensitivity at detecting action potentials in muscle fibers compared to GFP ( $\Delta F/F_0 = 7.1\%$  versus  $3.6\%$ , respectively, per 100 mV change in membrane potential).<sup>83</sup> Further screening of FP-PDA pairs resulted in hVOS 2.0, in which the fluorescence reporter cerulean fluorescent protein (CeFP) is sandwiched between an N-terminal GAP43 motif and a C-terminal truncated h-ras motif (GAP43-CeFP-t-h-ras). When expressed in PC12 cells, hVOS 2.0 has 3-fold higher voltage sensitivity compared to the original hVOS ( $\Delta F/F_0 = 26\%$  versus  $7.1\%$ , respectively, per 100 mV change in membrane potential); in cultured hippocampal neurons, hVOS 2.0 reports a  $10\% \Delta F/F_0$  change in response to an evoked action potential.<sup>84</sup> Moreover, these CeFP-based hVOS sensors can clearly resolve individual action potentials and their propagation at the circuit level in mouse brain slices.<sup>85,86</sup> Because the DPA molecules are embedded within the plasma membrane and translocate in response to a change in membrane potential, their presence increases the membrane capacitance.<sup>87</sup> In principle, this could reduce the neuron's excitability by affecting the initiation and/or propagation of action potentials.<sup>88</sup> Therefore, when used in mammalian neurons, the concentration of DPA should not exceed  $10 \mu\text{M}$ .<sup>81,89</sup>

An alternative strategy for generating FRET-based hybrid voltage indicators involves the use of microbial rhodopsins. These membrane proteins absorb intensely in the visible range, whose spectra depends on the membrane potential, a phenomenon known as electrochromism.<sup>8</sup> In microbial rhodopsins, a retinal chromophore is covalently linked to a lysine side chain via Schiff base. Electrochromism arises when the transmembrane electric field affects the energy landscape of the Schiff base protonation, thus shifting the absorption spectra.<sup>90</sup> In the past, we and others have capitalized on this effect to develop FRET-based voltage indicators by fusing FP donors to rhodopsin quenchers (called eFRET or FRET-opsin sensors).<sup>8,91,92</sup> Membrane potential modulates the degree of FRET energy transfer in these indicators, with a voltage sensitivity approaching  $18\% \Delta F/F_0$  per 100 mV. Theoretical analysis predicts that the voltage sensitivity of an eFRET

indicator is directly proportional to its baseline FRET efficiency,<sup>8</sup> suggesting that the sensor's sensitivity can be further increased by replacing the FP donor with a small-molecule fluorophore, which shortens the donor–acceptor distance. Indeed, our lab have recently employed this hybrid approach to develop a palette of FlareFRET (fluorophore ligation-assisted rhodopsin eFRET) indicators with submillisecond response kinetics.<sup>93</sup> We applied various site-specific protein labeling techniques, including HaloTag, SNAP-tag, and enzyme-mediated probe incorporation,<sup>94</sup> to ligate fluorophores to a rhodopsin protein. The most sensitive of this series, called Flare1, is an orange-colored indicator with  $35\% \Delta F/F_0$  per 100 mV voltage change in HEK293T cells, which is approximately twice as sensitive as FP-based eFRET voltage indicators (Figure 3C).<sup>93</sup> Because the chemical conjugation technique used to construct Flare1 requires copper-catalyzed click reaction, which is toxic to neurons, this method has not yet been extended to voltage imaging in neurons or in vivo. Future developments employing milder conjugation chemistry are underway.

The tetrahelical transmembrane domain of the voltage-sensing phosphatase (VSP) has also been used to generate hybrid voltage indicators. In VSP, a voltage-dependent conformational change in the fourth transmembrane helix shifts the position of its phosphatase effector, allosterically activating the enzyme. To report this conformational change, a series of genetically encoded voltage indicators was generated by fusing an FP to the VSP's transmembrane voltage-sensing domain (VSD).<sup>95</sup> In 2013, Tsutsui et al. replaced the FP with a synthetic fluorophore, using the rationale that these small molecules are more solvent-accessible than the chromophore that sits inside the FP's  $\beta$ -barrel structure and are therefore more sensitive to changes in the environment. In their study, the authors chose tetramethylrhodamine (TMR) as the small-molecule fluorophore, which was introduced in the form of a HaloTag ligand (Figure 3D). The resulting hybrid indicator, VSD-HaloTag-TMR, was capable of sensing a change in membrane potential with sensitivity of  $\sim 2.5\% \Delta F/F_0$  per 100 mV. Interestingly, their hybrid sensor had faster response kinetics compared to VSD-FP reporters.<sup>96</sup>

Another interesting variant of VSP-derived voltage indicators was produced by the introduction of a bioluminescent reporter. Recently, Nagai et al. fused NanoLuc and Venus to the N-terminus and C-terminus, respectively, of the VSD R217Q mutant to generate a BRET-based sensor for measuring voltage-induced conformational changes.<sup>97</sup> When expressed in HEK293T cells, this indicator, called LOTUS-V, has a  $21\%$  change in BRET ratio for each 100 mV change in membrane potential (Figure 3E).<sup>97</sup> Since LOTUS-V does not require excitation light illumination, it is possible to pair it with other optical perturbation strategies. For example, LOTUS-V has successfully detected voltage changes caused by multiple optogenetic actuators (Chr2 H134R and eNpHR3.0) in cultured PC12 cells.<sup>97</sup> In comparison, it is challenging to achieve this with most fluorescent voltage indicators, whose excitation spectra overlap with the action spectra of optogenetic tools.<sup>6</sup>

## CONCLUSIONS AND FUTURE PERSPECTIVES

In the past few decades, the neuroscience research community has benefited greatly from the growing toolbox of optical probes, which is dominated, at least currently, by fluorescent protein-based indicators. The popularity of fluorescent proteins stems largely from the fact that they are genetically encoded

and can be measured using a standard fluorescence microscope. Future generations of indicators must inherit these advantages while overcoming some of the weaknesses inherent to fluorescent proteins, including their size, photophysical properties, and dynamic range for sensing analytes. The hybrid indicators and bioluminescent sensors discussed in this Review could potentially fit for this role, yet a number of obstacles must be overcome to reach this goal. Below, we discuss existing challenges for hybrid indicators and bioluminescent sensors, and directions for future improvements.

Chemical probes are the core component of all hybrid sensors. While these synthetic fluorophores are often brighter and more photostable than conventional fluorescent proteins, they are not genetically encoded and require delivery in cell culture, tissue preparations and even intact brain. At the present stage, the vast majority of hybrid sensors have only been demonstrated in cell culture (see Table 1). Tissue delivery is often much less efficient due to both slowed diffusion and elimination from cells through active transport, which is a common problem for all small molecule dye imaging. One solution to this problem is to apply prolonged incubation with chemical probes during the imaging experiment, which often leads to higher background noise from unconjugated free probe. To reduce unwanted background and to improve the SNR, one could employ a fluorogenic labeling system.<sup>98</sup> For instance, the recently introduced fluorogenic Janelia Fluor dye JF<sub>585</sub> exhibits 78-fold increase in fluorescence upon conjugation with HaloTag protein, which has enabled specific labeling of mouse cortical neurons in layer 4 and layer 5 in vivo.<sup>99</sup>

Small molecule toxicity is another concern. Since exogenous chemical probes and their metabolites are potentially toxic to cells (e.g., FAsH and ReAsH contain toxic arsenic), it is important to include control experiments to show that probe incubation does not affect physiology, particularly for in vivo labeling. All fluorophores, including fluorescent proteins, generate toxic ROS to some extent upon light illumination. For many fluorescent proteins, their rigid  $\beta$ -barrel structure provides a cage that shields oxygen molecules away from the chromophore, thus reducing phototoxicity.<sup>100</sup> Without such protection, small molecule dyes tend to have higher rates of phototoxicity and photobleaching. Light illumination also inevitably excites endogenous chromophores in the tissue, causing additional phototoxicity. Together, these obstacles put a premium on the design and synthesis of fluorophores with high brightness and photostability. With respect to the color spectrum, probes with a far-red emission spectrum are more suitable for in vivo applications, because photochemical toxicity is attenuated by >100-fold at 640 nm than at 488 nm.<sup>101</sup> Optical scattering is also reduced at longer wavelengths.<sup>102</sup>

In addition to better probes, more versatile genetically encoded scaffolds are needed to detect analytes. So far, the majority of protein scaffolds in hybrid neurotransmitter sensors have been GPCRs, which specifically recognize an array of neurotransmitters and neuromodulators, including small molecule chemicals (e.g., using adrenergic<sup>20,21</sup> or muscarinic receptors<sup>22–24</sup>) and peptides (e.g., using the angiotensin II receptor<sup>103</sup> or parathyroid hormone receptor<sup>25</sup>). While these endogenous receptors constitute a convenient starting point for engineering, they can be complicated by oligomerization (GPCRs are dimers and Cys-loop receptors are pentamers) and potential crosstalks to cellular signaling pathways. One must take care to avoid affecting the physiology due to receptor overexpression, for example, by truncating the cytosolic domain

of GPCRs to prevent interactions with endogenous effector proteins, or by using GPCRs from different species. Looking beyond GPCRs, transporters—particularly those located in the plasma membrane—are promising scaffolds for developing transmitter sensors, although this application has not yet been explored in detail.

As a bridge between a rich palette of chemical fluorophores and versatile protein scaffolds, the conjugation chemistry is of paramount importance for hybrid indicators. An ideal labeling method should provide high specificity (i.e., no off-target signal), fast reaction kinetics (preferably within minutes), and low toxicity (i.e., avoid using toxic catalysts or generating toxic byproducts). To this end, a number of self-labeled tags and bio-orthogonal reactions have been developed. For example, fluorogenic SNAP-tag ligands with reaction rate constants reaching  $12\,000\text{ M}^{-1}\text{ s}^{-1}$  have been developed.<sup>104</sup> In addition, for these methods to be widely applicable, it is important to reduce the cost for fluorophores and labeling reagents, because the conjugation reactions often consume expensive, non-regenerative chemical probes.

With respect to bioluminescent indicators, one of the major challenges lies in the limited photon flux due to slow luciferase turnover rate. For this reason, bioluminescent imaging is often performed at slow frame rates (e.g., >20–30 ms/frame for voltage imaging),<sup>97</sup> which reduces the temporal resolution of the method. In terms of spatial resolution, bioluminescent imaging in vivo often does not distinguish individual cells in a densely labeled population. These limitations have partially offset the advantages of bioluminescence imaging over fluorescence imaging, particularly when modern, bright FP-based indicators with ultrahigh SNR already has provided reduced phototoxicity.

Future development of bioluminescent indicators should focus on increasing the luciferase turnover rate, luminescence quantum yield, and shifting the spectrum to the far-red. NLuc, the smaller and more robust version of luciferase, is justifiably the top choice today. Improved NLuc and luciferin pairs with more red-shifted and brighter bioluminescence were recently reported by Ai and colleagues;<sup>57</sup> these new pairs also provide the opportunity to build new BRET-based indicators for sensing neurotransmitters. The far-red spectrum of substrates not only opens the door for generating multiplex indicators, but it also pushes the envelope for bioluminescence-based sensing from in vitro imaging to robust in vivo applications in living systems.

## ■ ASSOCIATED CONTENT

### 📄 Supporting Information

The Supporting Information is available free of charge on the ACS Publications website at DOI: [10.1021/acscchemneuro.7b00455](https://doi.org/10.1021/acscchemneuro.7b00455).

Photophysical properties and kinetics of the hybrid and bioluminescent indicators (PDF)

## ■ AUTHOR INFORMATION

### Corresponding Authors

\*E-mail: [yulongli@pku.edu.cn](mailto:yulongli@pku.edu.cn).

\*E-mail: [zoupeng@pku.edu.cn](mailto:zoupeng@pku.edu.cn).

### ORCID

Peng Zou: 0000-0002-9798-5242

## Author Contributions

A.W. and J.F. contributed equally. J.F. and Y.L. wrote the section on neurotransmitter sensors. A.W. and P.Z. wrote the sections on metal ion, ROS/RNS, and membrane potential sensors. All authors wrote the introduction, conclusions, and future perspectives together.

## Funding

A.W., J.F., Y.L., and P.Z. were supported by the Peking-Tsinghua Center for Life Sciences, the PKU-IDG/McGovern Institute for Brain Research. A.W. and P.Z. were supported by the National Natural Science Foundation of China (Grants 21673009, 21727806). Y.L. and P.Z. were supported by the National Thousand Young Talents Award. J.S. and Y.L. were supported by the National Natural Science Foundation of China (Grant 31671118) and the National Basic Research Program of China (973 Program, Project Number 2015CB856402).

## Notes

The authors declare no competing financial interest.

## REFERENCES

- (1) Chalfie, M., Tu, Y., Euskirchen, G., Ward, W. W., and Prasher, D. C. (1994) Green fluorescent protein as a marker for gene expression. *Science* 263 (5148), 802–5.
- (2) Heim, R., Cubitt, A. B., and Tsien, R. Y. (1995) Improved green fluorescence. *Nature* 373 (6516), 663–4.
- (3) Tsien, R. Y. (1998) The green fluorescent protein. *Annu. Rev. Biochem.* 67, 509–44.
- (4) Liang, R., Broussard, G. J., and Tian, L. (2015) Imaging chemical neurotransmission with genetically encoded fluorescent sensors. *ACS Chem. Neurosci.* 6 (1), 84–93.
- (5) Tian, L., Hires, S. A., and Looger, L. L. (2012) Imaging neuronal activity with genetically encoded calcium indicators. *Cold Spring Harbor Protocols* 2012 (6), 647–56.
- (6) Xu, Y., Zou, P., and Cohen, A. E. (2017) Voltage imaging with genetically encoded indicators. *Curr. Opin. Chem. Biol.* 39, 1–10.
- (7) Stennett, E. M., Ciuba, M. A., and Levitus, M. (2014) Photophysical processes in single molecule organic fluorescent probes. *Chem. Soc. Rev.* 43 (4), 1057–75.
- (8) Zou, P., Zhao, Y., Douglass, A. D., Hochbaum, D. R., Brinks, D., Werley, C. A., Harrison, D. J., Campbell, R. E., and Cohen, A. E. (2014) Bright and fast multicoloured voltage reporters via electrochromic FRET. *Nat. Commun.* 5, 4625.
- (9) Shcherbakova, D. M., and Verkhusha, V. V. (2013) Near-infrared fluorescent proteins for multicolor in vivo imaging. *Nat. Methods* 10 (8), 751–4.
- (10) Žiburkus, J., Cressman, J. R., and Schiff, S. J. (2013) Seizures as imbalanced up states: excitatory and inhibitory conductances during seizure-like events. *J. Neurophysiol.* 109 (5), 1296–1306.
- (11) van Spronsen, M., and Hoogenraad, C. C. (2010) Synapse Pathology in Psychiatric and Neurologic Disease. *Curr. Neurol. Neurosci. Rep.* 10 (3), 207–214.
- (12) Namiki, S., Sakamoto, H., Iinuma, S., Iino, M., and Hirose, K. (2007) Optical glutamate sensor for spatiotemporal analysis of synaptic transmission. *Eur. J. Neurosci.* 25 (8), 2249–59.
- (13) Abele, R., Keinanen, K., and Madden, D. R. (2000) Agonist-induced isomerization in a glutamate receptor ligand-binding domain. A kinetic and mutagenetic analysis. *J. Biol. Chem.* 275 (28), 21355–63.
- (14) Bergles, D. E., Diamond, J. S., and Jahr, C. E. (1999) Clearance of glutamate inside the synapse and beyond. *Curr. Opin. Neurobiol.* 9 (3), 293–8.
- (15) Okubo, Y., Sekiya, H., Namiki, S., Sakamoto, H., Iinuma, S., Yamasaki, M., Watanabe, M., Hirose, K., and Iino, M. (2010) Imaging extrasynaptic glutamate dynamics in the brain. *Proc. Natl. Acad. Sci. U. S. A.* 107 (14), 6526–31.
- (16) Okubo, Y., and Iino, M. (2011) Visualization of glutamate as a volume transmitter. *J. Physiol.* 589 (3), 481–488.
- (17) Takikawa, K., Asanuma, D., Namiki, S., Sakamoto, H., Ariyoshi, T., Kimpara, N., and Hirose, K. (2014) High-Throughput Development of a Hybrid-Type Fluorescent Glutamate Sensor for Analysis of Synaptic Transmission. *Angew. Chem., Int. Ed.* 53 (49), 13439–13443.
- (18) Vilardaga, J.-P., Bunemann, M., Krasel, C., Castro, M., and Lohse, M. J. (2003) Measurement of the millisecond activation switch of G protein-coupled receptors in living cells. *Nat. Biotechnol.* 21 (7), 807–812.
- (19) Adams, S. R., Campbell, R. E., Gross, L. A., Martin, B. R., Walkup, G. K., Yao, Y., Llopis, J., and Tsien, R. Y. (2002) New Biarsenical Ligands and Tetracysteine Motifs for Protein Labeling in Vitro and in Vivo: Synthesis and Biological Applications. *J. Am. Chem. Soc.* 124 (21), 6063–6076.
- (20) Hoffmann, C., Gaietta, G., Bunemann, M., Adams, S. R., Oberdorff-Maass, S., Behr, B., Vilardaga, J.-P., Tsien, R. Y., Ellisman, M. H., and Lohse, M. J. (2005) A FRET-based approach to determine G protein-coupled receptor activation in living cells. *Nat. Methods* 2 (3), 171–176.
- (21) Nakanishi, J., Takarada, T., Yunoki, S., Kikuchi, Y., and Maeda, M. (2006) FRET-based monitoring of conformational change of the beta(2) adrenergic receptor in living cells. *Biochem. Biophys. Res. Commun.* 343 (4), 1191–1196.
- (22) Maier-Peuschel, M., Frölich, N., Dees, C., Hommers, L. G., Hoffmann, C., Nikolaev, V. O., and Lohse, M. J. (2010) A Fluorescence Resonance Energy Transfer-based M(2) Muscarinic Receptor Sensor Reveals Rapid Kinetics of Allosteric Modulation. *J. Biol. Chem.* 285 (12), 8793–8800.
- (23) Ziegler, N., Bätz, J., Zabel, U., Lohse, M. J., and Hoffmann, C. (2011) FRET-based sensors for the human M1-, M3-, and M5-acetylcholine receptors. *Bioorg. Med. Chem.* 19 (3), 1048–1054.
- (24) Chang, S., and Ross, E. M. (2012) Activation Biosensor for G Protein-Coupled Receptors: A FRET-Based m1Muscarinic Activation Sensor That Regulates Gq. *PLoS One* 7 (9), e45651.
- (25) Zürn, A., Klenk, C., Zabel, U., Reiner, S., Lohse, M. J., and Hoffmann, C. (2010) Site-Specific, Orthogonal Labeling of Proteins in Intact Cells with Two Small Biarsenical Fluorophores. *Bioconjugate Chem.* 21 (5), 853–859.
- (26) Brun, M. A., Griss, R., Reymond, L., Tan, K. T., Piguet, J., Peters, R. J., Vogel, H., and Johnsson, K. (2011) Semisynthesis of fluorescent metabolite sensors on cell surfaces. *J. Am. Chem. Soc.* 133 (40), 16235–42.
- (27) Masharina, A., Reymond, L., Maurel, D., Umezawa, K., and Johnsson, K. (2012) A fluorescent sensor for GABA and synthetic GABA(B) receptor ligands. *J. Am. Chem. Soc.* 134 (46), 19026–34.
- (28) Brun, M. A., Tan, K. T., Griss, R., Kielkowska, A., Reymond, L., and Johnsson, K. (2012) A semisynthetic fluorescent sensor protein for glutamate. *J. Am. Chem. Soc.* 134 (18), 7676–8.
- (29) Brun, M. A., Tan, K.-T., Nakata, E., Hinner, M. J., and Johnsson, K. (2009) Semisynthetic Fluorescent Sensor Proteins Based on Self-Labeling Protein Tags. *J. Am. Chem. Soc.* 131 (16), 5873–5884.
- (30) Keppler, A., Gendreizig, S., Gronemeyer, T., Pick, H., Vogel, H., and Johnsson, K. (2003) A general method for the covalent labeling of fusion proteins with small molecules in vivo. *Nat. Biotechnol.* 21 (1), 86–89.
- (31) Gautier, A., Juillerat, A., Heinis, C., Correa, I. R., Jr., Kindermann, M., Beaufils, F., and Johnsson, K. (2008) An engineered protein tag for multiprotein labeling in living cells. *Chem. Biol.* 15 (2), 128–36.
- (32) Schena, A., and Johnsson, K. (2014) Sensing Acetylcholine and Anticholinesterase Compounds. *Angew. Chem., Int. Ed.* 53 (5), 1302–1305.
- (33) Doumazane, E., Scholler, P., Fabre, L., Zwier, J. M., Trinquet, E., Pin, J.-P., and Rondard, P. (2013) Illuminating the activation mechanisms and allosteric properties of metabotropic glutamate receptors. *Proc. Natl. Acad. Sci. U. S. A.* 110 (15), E1416–E1425.
- (34) Angers, S., Salahpour, A., Joly, E., Hilairiet, S., Chelsky, D., Dennis, M., and Bouvier, M. (2000) Detection of  $\beta(2)$ -adrenergic

- receptor dimerization in living cells using bioluminescence resonance energy transfer (BRET). *Proc. Natl. Acad. Sci. U. S. A.* 97 (7), 3684–3689.
- (35) Hamdan, F. F., Audet, M., Garneau, P., Pelletier, J., and Bouvier, M. (2005) High-Throughput Screening of G Protein-Coupled Receptor Antagonists Using a Bioluminescence Resonance Energy Transfer 1-Based  $\beta$ -Arrestin2 Recruitment Assay. *J. Biomol. Screening* 10 (5), 463–475.
- (36) Kono, M., Conlon, E. G., Lux, S. Y., Yanagida, K., Hla, T., and Proia, R. L. (2017) Bioluminescence imaging of G protein-coupled receptor activation in living mice. *Nat. Commun.* 8 (1), 1163.
- (37) Griss, R., Schena, A., Reymond, L., Patiny, L., Werner, D., Tinberg, C. E., Baker, D., and Johnsson, K. (2014) Bioluminescent sensor proteins for point-of-care therapeutic drug monitoring. *Nat. Chem. Biol.* 10 (7), 598–603.
- (38) Hattori, M., Tanaka, M., Takakura, H., Aoki, K., Miura, K., Anzai, T., and Ozawa, T. (2013) Analysis of temporal patterns of GPCR-beta-arrestin interactions using split luciferase-fragment complementation. *Mol. BioSyst.* 9 (5), 957–964.
- (39) Berridge, M. J., Lipp, P., and Bootman, M. D. (2000) The versatility and universality of calcium signalling. *Nat. Rev. Mol. Cell Biol.* 1 (1), 11–21.
- (40) Augustine, G. J., Santamaria, F., and Tanaka, K. (2003) Local calcium signaling in neurons. *Neuron* 40 (2), 331–46.
- (41) Grynkiewicz, G., Poenie, M., and Tsien, R. Y. (1985) A new generation of Ca<sup>2+</sup> indicators with greatly improved fluorescence properties. *J. Biol. Chem.* 260 (6), 3440–50.
- (42) Bannwarth, M., Correa, I. R., Sztrzytey, M., Pouvreau, S., Fellay, C., Aebischer, A., Royer, L., Rios, E., and Johnsson, K. (2009) Indo-1 derivatives for local calcium sensing. *ACS Chem. Biol.* 4 (3), 179–190.
- (43) Kamiya, M., and Johnsson, K. (2010) Localizable and highly sensitive calcium indicator based on a BODIPY fluorophore. *Anal. Chem.* 82 (15), 6472–9.
- (44) Ruggiu, A. A., Bannwarth, M., and Johnsson, K. (2010) Fura-2FF-based calcium indicator for protein labeling. *Org. Biomol. Chem.* 8 (15), 3398–401.
- (45) Chen, T. W., Wardill, T. J., Sun, Y., Pulver, S. R., Renninger, S. L., Baohan, A., Schreiter, E. R., Kerr, R. A., Orger, M. B., Jayaraman, V., Looger, L. L., Svoboda, K., and Kim, D. S. (2013) Ultrasensitive fluorescent proteins for imaging neuronal activity. *Nature* 499 (7458), 295–300.
- (46) Brini, M., Marsault, R., Bastianutto, C., Alvarez, J., Pozzan, T., and Rizzuto, R. (1995) Transfected aequorin in the measurement of cytosolic Ca<sup>2+</sup> concentration ([Ca<sup>2+</sup>]<sub>c</sub>). A critical evaluation. *J. Biol. Chem.* 270 (17), 9896–903.
- (47) Baubet, V., Le Mouellic, H., Campbell, A. K., Lucas-Meunier, E., Fossier, P., and Brulet, P. (2000) Chimeric green fluorescent protein-aequorin as bioluminescent Ca<sup>2+</sup> reporters at the single-cell level. *Proc. Natl. Acad. Sci. U. S. A.* 97 (13), 7260–5.
- (48) Shimomura, O., Kishi, Y., and Inouye, S. (1993) The relative rate of aequorin regeneration from apoaequorin and coelenterazine analogues. *Biochem. J.* 296 (3), 549–51.
- (49) Loening, A. M., Fenn, T. D., Wu, A. M., and Gambhir, S. S. (2006) Consensus guided mutagenesis of Renilla luciferase yields enhanced stability and light output. *Protein Eng., Des. Sel.* 19 (9), 391–400.
- (50) Saito, K., Hatsugai, N., Horikawa, K., Kobayashi, K., Matsu-Ura, T., Mikoshiba, K., and Nagai, T. (2010) Auto-luminescent genetically-encoded ratiometric indicator for real-time Ca<sup>2+</sup> imaging at the single cell level. *PLoS One* 5 (4), e9935.
- (51) Saito, K., Chang, Y. F., Horikawa, K., Hatsugai, N., Higuchi, Y., Hashida, M., Yoshida, Y., Matsuda, T., Arai, Y., and Nagai, T. (2012) Luminescent proteins for high-speed single-cell and whole-body imaging. *Nat. Commun.* 3, 1262.
- (52) Takai, A., Nakano, M., Saito, K., Haruno, R., Watanabe, T. M., Ohyanagi, T., Jin, T., Okada, Y., and Nagai, T. (2015) Expanded palette of Nano-lanterns for real-time multicolor luminescence imaging. *Proc. Natl. Acad. Sci. U. S. A.* 112 (14), 4352–6.
- (53) Suzuki, K., Kimura, T., Shinoda, H., Bai, G., Daniels, M. J., Arai, Y., Nakano, M., and Nagai, T. (2016) Five colour variants of bright luminescent protein for real-time multicolour bioimaging. *Nat. Commun.* 7, 13718.
- (54) Thestrup, T., Litzlbauer, J., Bartholomaeus, I., Mues, M., Russo, L., Dana, H., Kovalchuk, Y., Liang, Y., Kalamakis, G., Laukat, Y., Becker, S., Witte, G., Geiger, A., Allen, T., Rome, L. C., Chen, T. W., Kim, D. S., Garaschuk, O., Griesinger, C., and Griesbeck, O. (2014) Optimized ratiometric calcium sensors for functional in vivo imaging of neurons and T lymphocytes. *Nat. Methods* 11 (2), 175–82.
- (55) Hall, M. P., Unch, J., Binkowski, B. F., Valley, M. P., Butler, B. L., Wood, M. G., Otto, P., Zimmerman, K., Vidugiris, G., Machleidt, T., Robers, M. B., Benink, H. A., Eggers, C. T., Slater, M. R., Meisenheimer, P. L., Klaubert, D. H., Fan, F., Encell, L. P., and Wood, K. V. (2012) Engineered luciferase reporter from a deep sea shrimp utilizing a novel imidazopyrazinone substrate. *ACS Chem. Biol.* 7 (11), 1848–57.
- (56) Yang, J., Cumberbatch, D., Centanni, S., Shi, S. Q., Winder, D., Webb, D., and Johnson, C. H. (2016) Coupling optogenetic stimulation with NanoLuc-based luminescence (BRET) Ca<sup>++</sup> sensing. *Nat. Commun.* 7, 13268.
- (57) Yeh, H. W., Karmach, O., Ji, A., Carter, D., Martins-Green, M. M., and Ai, H. W. (2017) Red-shifted luciferase-luciferin pairs for enhanced bioluminescence imaging. *Nat. Methods* 14 (10), 971–974.
- (58) Takeda, A. (2011) Zinc signaling in the hippocampus and its relation to pathogenesis of depression. *Mol. Neurobiol.* 44 (2), 166–74.
- (59) Takeda, A., Fuke, S., Ando, M., and Oku, N. (2009) Positive modulation of long-term potentiation at hippocampal CA1 synapses by low micromolar concentrations of zinc. *Neuroscience* 158 (2), 585–591.
- (60) Takeda, A., Takada, S., Nakamura, M., Suzuki, M., Tamano, H., Ando, M., and Oku, N. (2011) Transient increase in Zn<sup>2+</sup> in hippocampal CA1 pyramidal neurons causes reversible memory deficit. *PLoS One* 6 (12), e28615.
- (61) Los, G. V., Encell, L. P., McDougall, M. G., Hartzell, D. D., Karassina, N., Zimprich, C., Wood, M. G., Learish, R., Ohana, R. F., Urh, M., Simpson, D., Mendez, J., Zimmerman, K., Otto, P., Vidugiris, G., Zhu, J., Darzins, A., Klaubert, D. H., Bulleit, R. F., and Wood, K. V. (2008) HaloTag: a novel protein labeling technology for cell imaging and protein analysis. *ACS Chem. Biol.* 3 (6), 373–82.
- (62) Tomat, E., Nolan, E. M., Jaworski, J., and Lippard, S. J. (2008) Organelle-specific zinc detection using zinpyr-labeled fusion proteins in live cells. *J. Am. Chem. Soc.* 130 (47), 15776–7.
- (63) Li, D., Chen, S., Bellomo, E. A., Tarasov, A. I., Kaut, C., Rutter, G. A., and Li, W. H. (2011) Imaging dynamic insulin release using a fluorescent zinc indicator for monitoring induced exocytotic release (ZIMIR). *Proc. Natl. Acad. Sci. U. S. A.* 108 (52), 21063–8.
- (64) Li, D., Liu, L., and Li, W. H. (2015) Genetic targeting of a small fluorescent zinc indicator to cell surface for monitoring zinc secretion. *ACS Chem. Biol.* 10 (4), 1054–63.
- (65) Aper, S. J., Dierickx, P., and Merckx, M. (2016) Dual Readout BRET/FRET Sensors for Measuring Intracellular Zinc. *ACS Chem. Biol.* 11 (10), 2854–2864.
- (66) Olguin-Albuerno, M., and Moran, J. (2015) ROS produced by NOX2 control in vitro development of cerebellar granule neurons development. *ASN Neuro* 7 (2), 175909141557871.
- (67) Kamsler, A. S. M. (2003) Hydrogen peroxide modulation of synaptic plasticity. *J. Neurosci.* 23, 269–276.
- (68) Avshalumov, M. V., Chen, B. T., and Rice, M. E. (2000) Mechanisms underlying H<sub>2</sub>O<sub>2</sub>-mediated inhibition of synaptic transmission in rat hippocampal slices. *Brain Res.* 882 (1), 86–94.
- (69) Avshalumov, M. V., Chen, B. T., Koós, T., Tepper, J. M., and Rice, M. E. (2005) Endogenous Hydrogen Peroxide Regulates the Excitability of Midbrain Dopamine Neurons via ATP-Sensitive Potassium Channels. *J. Neurosci.* 25 (17), 4222.
- (70) Nathan, C. (1992) Nitric oxide as a secretory product of mammalian cells. *FASEB J.* 6 (12), 3051–64.
- (71) Gibbs, S. M. (2003) Regulation of neuronal proliferation and differentiation by nitric oxide. *Mol. Neurobiol.* 27 (2), 107–120.

- (72) Hölscher, C. (1997) Nitric oxide, the enigmatic neuronal messenger: its role in synaptic plasticity. *Trends Neurosci.* 20 (7), 298–303.
- (73) Srikun, D., Albers, A. E., Nam, C. I., Iavarone, A. T., and Chang, C. J. (2010) Organelle-targetable fluorescent probes for imaging hydrogen peroxide in living cells via SNAP-Tag protein labeling. *J. Am. Chem. Soc.* 132 (12), 4455–65.
- (74) Wang, C., Song, X., Han, Z., Li, X., Xu, Y., and Xiao, Y. (2016) Monitoring Nitric Oxide in Subcellular Compartments by Hybrid Probe Based on Rhodamine Spiroactam and SNAP-tag. *ACS Chem. Biol.* 11 (7), 2033–2040.
- (75) Takakura, H., Kojima, R., Kamiya, M., Kobayashi, E., Komatsu, T., Ueno, T., Terai, T., Hanaoka, K., Nagano, T., and Urano, Y. (2015) New class of bioluminogenic probe based on bioluminescent enzyme-induced electron transfer: BioLE<sup>T</sup>. *J. Am. Chem. Soc.* 137 (12), 4010–3.
- (76) Kojima, R., Takakura, H., Kamiya, M., Kobayashi, E., Komatsu, T., Ueno, T., Terai, T., Hanaoka, K., Nagano, T., and Urano, Y. (2015) Development of a Sensitive Bioluminogenic Probe for Imaging Highly Reactive Oxygen Species in Living Rats. *Angew. Chem., Int. Ed.* 54 (49), 14768–71.
- (77) Hinner, M. J., Hubener, G., and Fromherz, P. (2006) Genetic targeting of individual cells with a voltage-sensitive dye through enzymatic activation of membrane binding. *ChemBioChem* 7 (3), 495–505.
- (78) Ng, D. N., and Fromherz, P. (2011) Genetic targeting of a voltage-sensitive dye by enzymatic activation of phosphonooxymethylammonium derivative. *ACS Chem. Biol.* 6 (5), 444–51.
- (79) Gonzalez, J. E., and Tsien, R. Y. (1995) Voltage sensing by fluorescence resonance energy transfer in single cells. *Biophys. J.* 69 (4), 1272–80.
- (80) Siegel, M. S., and Isacoff, E. Y. (1997) A genetically encoded optical probe of membrane voltage. *Neuron* 19 (4), 735–41.
- (81) Chanda, B., Blunck, R., Faria, L. C., Schweizer, F. E., Mody, I., and Bezanilla, F. (2005) A hybrid approach to measuring electrical activity in genetically specified neurons. *Nat. Neurosci.* 8 (11), 1619–26.
- (82) Weigel, S., Flisikowska, T., Schnieke, A., and Luksch, H. (2014) Hybrid voltage sensor imaging of eGFP-F expressing neurons in chicken midbrain slices. *J. Neurosci. Methods* 233, 28–33.
- (83) DiFranco, M., Capote, J., Quinonez, M., and Vergara, J. L. (2007) Voltage-dependent dynamic FRET signals from the transverse tubules in mammalian skeletal muscle fibers. *J. Gen. Physiol.* 130 (6), 581–600.
- (84) Wang, D., Zhang, Z., Chanda, B., and Jackson, M. B. (2010) Improved probes for hybrid voltage sensor imaging. *Biophys. J.* 99 (7), 2355–65.
- (85) Ghitani, N., Bayguinov, P. O., Ma, Y., and Jackson, M. B. (2015) Single-trial imaging of spikes and synaptic potentials in single neurons in brain slices with genetically encoded hybrid voltage sensor. *J. Neurophysiol.* 113 (4), 1249–59.
- (86) Wang, D., McMahon, S., Zhang, Z., and Jackson, M. B. (2012) Hybrid voltage sensor imaging of electrical activity from neurons in hippocampal slices from transgenic mice. *J. Neurophysiol.* 108 (11), 3147–60.
- (87) Fernandez, J. M., Taylor, R. E., and Bezanilla, F. (1983) Induced capacitance in the squid giant axon. Lipophilic ion displacement currents. *J. Gen. Physiol.* 82 (3), 331–46.
- (88) Sjulson, L., and Miesenbock, G. (2008) Rational optimization and imaging in vivo of a genetically encoded optical voltage reporter. *J. Neurosci.* 28 (21), 5582–93.
- (89) Bradley, J., Luo, R., Otis, T. S., and DiGregorio, D. A. (2009) Submillisecond optical reporting of membrane potential in situ using a neuronal tracer dye. *J. Neurosci.* 29 (29), 9197–209.
- (90) Kralj, J. M., Hochbaum, D. R., Douglass, A. D., and Cohen, A. E. (2011) Electrical spiking in *Escherichia coli* probed with a fluorescent voltage-indicating protein. *Science* 333 (6040), 345–8.
- (91) Gong, Y., Wagner, M. J., Zhong, L. J., and Schnitzer, M. J. (2014) Imaging neural spiking in brain tissue using FRET-opsin protein voltage sensors. *Nat. Commun.* 5, 3674.
- (92) Gong, Y., Huang, C., Li, J. Z., Grewe, B. F., Zhang, Y., Eismann, S., and Schnitzer, M. J. (2015) High-speed recording of neural spikes in awake mice and flies with a fluorescent voltage sensor. *Science* 350 (6266), 1361–6.
- (93) Xu, Y., Peng, L., Wang, S., Wang, A., Ma, R., Zhou, Y., Yang, J., Sun, D. E., Lin, W., Chen, X., and Zou, P. (2018) Hybrid Indicators for Fast and Sensitive Voltage Imaging. *Angew. Chem., Int. Ed.*, DOI: 10.1002/anie.201712614.
- (94) Uttamapinant, C., Sanchez, M. I., Liu, D. S., Yao, J. Z., and Ting, A. Y. (2013) Site-specific protein labeling using PRIME and chelation-assisted click chemistry. *Nat. Protoc.* 8 (8), 1620–1634.
- (95) Peng, L., Xu, Y., and Zou, P. (2017) Genetically-encoded voltage indicators. *Chin. Chem. Lett.* 28 (10), 1925–1928.
- (96) Tsutsui, H., Jinno, Y., Tomita, A., and Okamura, Y. (2013) Optically detected structural change in the N-terminal region of the voltage-sensor domain. *Biophys. J.* 105 (1), 108–15.
- (97) Inagaki, S., Tsutsui, H., Suzuki, K., Agetsuma, M., Arai, Y., Jinno, Y., Bai, G., Daniels, M. J., Okamura, Y., Matsuda, T., and Nagai, T. (2017) Genetically encoded bioluminescent voltage indicator for multi-purpose use in wide range of bioimaging. *Sci. Rep.* 7, 42398.
- (98) Arai, S., Yoon, S.-I., Murata, A., Takabayashi, M., Wu, X., Lu, Y., Takeoka, S., and Ozaki, M. (2011) Fluorescent “Turn-on” system utilizing a quencher-conjugated peptide for specific protein labeling of living cells. *Biochem. Biophys. Res. Commun.* 404 (1), 211–216.
- (99) Grimm, J. B., Muthusamy, A. K., Liang, Y., Brown, T. A., Lemon, W. C., Patel, R., Lu, R., Macklin, J. J., Keller, P. J., Ji, N., and Lavis, L. D. (2017) A general method to fine-tune fluorophores for live-cell and in vivo imaging. *Nat. Methods* 14 (10), 987–994.
- (100) Carpentier, P., Violot, S., Blanchoin, L., and Bourgeois, D. (2009) Structural basis for the phototoxicity of the fluorescent protein KillerRed. *FEBS Lett.* 583 (17), 2839–42.
- (101) Waldchen, S., Lehmann, J., Klein, T., van de Linde, S., and Sauer, M. (2015) Light-induced cell damage in live-cell super-resolution microscopy. *Sci. Rep.* 5, 15348.
- (102) Jacques, S. L. (2013) Optical properties of biological tissues: a review. *Phys. Med. Biol.* 58 (11), R37–61.
- (103) Szalai, B., Barkai, L., Turu, G., Szidonya, L., Várnai, P., and Hunyady, L. (2012) Allosteric interactions within the AT1 angiotensin receptor homodimer: Role of the conserved DRY motif. *Biochem. Pharmacol.* 84 (4), 477–485.
- (104) Sun, X., Zhang, A., Baker, B., Sun, L., Howard, A., Buswell, J., Maurel, D., Masharina, A., Johnsson, K., Noren, C. J., Xu, M. Q., and Correa, I. R., Jr. (2011) Development of SNAP-tag fluorogenic probes for wash-free fluorescence imaging. *ChemBioChem* 12 (14), 2217–26.